HHS Public Access

Author manuscript

*Obesity (Silver Spring)*. Author manuscript; available in PMC 2024 April 01.

Published in final edited form as:

*Obesity (Silver Spring)*. 2023 April ; 31(4): 1024–1037. doi:10.1002/oby.23692.

# *Gpr75*-deficient mice are protected from high fat diet-induced obesity

**Sakib Hossain**,

**Ankit Gilani**,

**Jonathan Pascale**,

**Elizabeth Villegas**,

**Danielle Diegisser**,

**Kevin Agostinucci**,

**Melissa-Maria Kulaprathazhe**,

**Ercument Dirice**,

**Victor Garcia**,

**Michal Laniado Schwartzman**

Department of Pharmacology, New York Medical College School of Medicine, Valhalla, NY

## Abstract

**Objective -—**We have identified GPR75 as the high affinity receptor of 20-hydroxyeicosatetraenoic acid (20-HETE), a vasoactive and pro-inflammatory lipid, and reported that mice overproducing 20-HETE develop insulin resistance when fed a high-fat diet (HFD), which was prevented by a 20-HETE receptor blocker. Simultaneously, a large-scale exome sequencing of 640,000 subjects identified association between loss of function *GPR75* variants and protection against obesity.

**Methods ——**Wild type and *Gpr75*-deficient mice were placed on HFD for 14 weeks and their obese phenotype was examined.

**Results -—**Male and female *Gpr75* null (KO) and heterozygous (HET) mice gained less weight than wild type (WT) when placed on HFD. KO mice maintained the same level of energy expenditures during HFD feeding, while WT showed a significant reduction in energy expenditure. Diet-driven adiposity and adipocyte hypertrophy were greatly lessened in *Gpr75*-deficient mice. HFD-fed KO mice did not develop insulin resistance. Adipose tissues from *Gpr75*-deficient mice had increased expression of thermogenic genes and decreased levels of inflammatory markers. Moreover, insulin signaling which was impaired in HFD-fed WT was unchanged in KO mice.

**CORRESPONDING AUTHOR:** Michal Laniado Schwartzman, Department of Pharmacology, New York Medical College, 15 Dana Road, Valhalla, NY 10595. Michal_Schwartzman@nymc.edu. Phone: +1-914-594-3116. Fax: +1-914-347-4956.

**DISCLOSURE:** The authors declared no conflict of interest

**Conclusions -—**These findings suggest that GPR75 is an important player in the control of metabolism and glucose homeostasis and a likely novel therapeutic target to combat obesity-driven metabolic disorders.

## Graphical Abstract

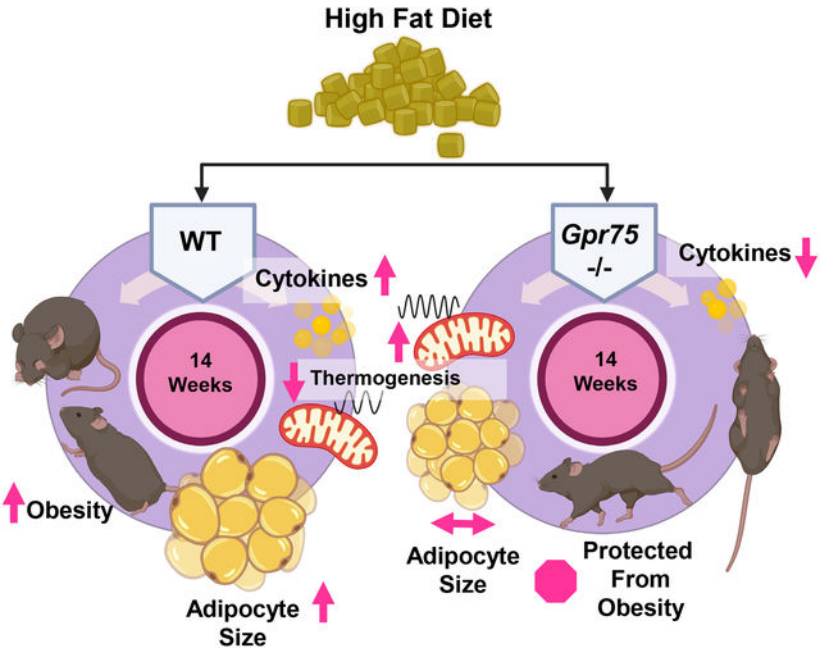


### Keywords

Obesity; Hyperglycemia; Insulin Resistance; Adiposity; Inflammation

## INTRODUCTION

Obesity (BMI ≥ 30) is linked to several prevalent and costly medical conditions including type 2 diabetes, hypertension, coronary heart disease, stroke and liver disease as well as increased disability and mortality. According to the CDC, from 2000 through 2018, the prevalence of obesity increased from 30.5% to 42.4%, whereas that of severe obesity (BMI ≥ 40) went from 4.7% to 9.2%. Obesity affects more than 80 million people and is expected to increase to over 50% of the US population by 2030 (https://www.cdc.gov/nchs/products/databriefs/db360.htm). Likewise, worldwide obesity has tripled since 1975. (https://www.who.int/news-room/fact-sheets/detail/obesity-and-overweight). Obesity is a highly polygenic and complex disorder resulting from the interactions between genes regulating food intake and energy expenditure with environmental and behavioral factors. It is estimated that up to 40% of variation in BMI can be explained by genetic factors. We have recently added to the long list of obesity genes, the orphan G-protein coupled receptor 75 (GPR75). A recent scientific consortium including our group uncovered several loss of function *GPR75* variants associated with leanness and protection from obesity. This finding matches results from *Gpr75* null mice which are protected from high-fat diet (HFD)-driven

adiposity and insulin resistance (1). The mechanisms underlying the contribution of GPR75 to obesity and associated pathologies are unknown.

GPR75 is currently classified as a class A orphan receptor that preferentially couples with $G_q\alpha$. There are a few studies suggesting that the chemokine CCL5 activates GPR75 via a $G_q\alpha$ protein-coupled PLC-mediated signal transduction pathway in cells overexpressing GPR75, pancreatic islets and neuroblastoma cell lines (2–4). However, no direct binding studies between CCL5 and GPR75 were documented in those studies and the pairing could not be repeated in a β-arrestin assay (5, 6). A recent study from our laboratory identified GPR75 as the receptor to which 20-hydroxyeicosatetraenoic acid (20-HETE), a bioactive lipid mediator formed by cytochrome P450 (CYP) monooxygenases, binds, and triggers its actions (7). We further provided strong evidence for high affinity binding of 20-HETE to GPR75 and the activation of GPR75(Gq) signaling by 20-HETE including stimulation of intracellular $Ca^{2+}$ accumulation and β-arrestin recruitment; all of which were negated by 20-HETE receptor blockers (8). Moreover, we showed that CCL5 binds to GPR75 but fails to activate its signaling. However, it blocked 20-HETE-mediated GPR75 activation (8).

Regarding obesity, plasma and tissue 20-HETE levels increased in animal models of obesity and metabolic syndrome and strongly correlated with BMI in humans (9–15). 20-HETE stimulates lipid accumulation during adipogenesis *in vitro* (16), and a role of 20-HETE in the pathogenesis of diabetes has been suggested (17, 18). We and others have shown that 20-HETE impairs insulin receptor signaling (19–21) and that overexpression of 20-HETE synthases (CYP4A12, CYP4F2) in mice is associated with exacerbated diet-driven weight gain, hyperglycemia and insulin resistance (20–22). Furthermore, using 20-HETE receptor blockers, we demonstrated causal relationships between 20-HETE and insulin resistance in HFD-driven obesity, and between 20-HETE levels and impaired insulin signaling in adipose tissue, skeletal muscles and liver (20, 21). In all, these studies suggest that 20-HETE-GPR75 pairing is the underlying mechanism of 20-HETE's contribution to obesity and its associated pathologies. The present study was undertaken to fully characterize the metabolic phenotype of *Gpr75* null mice when fed HFD and explore potential mechanisms by which GPR75 activation links to increased adiposity and decreased insulin sensitivity.

## METHODS

All experimental protocols were approved by the Institutional Animal Care and Use Committee in accordance with the National Institutes of Health Guidelines for the Care and Use of Laboratory Animals. *Gpr75* null mice were generated by Regeneron Pharmaceuticals using the VelociMouse technology (1). Male and female *Gpr75* null (KO), heterozygous (HET) and wild type (WT) mice were housed in static cages at room temperature (20–22°C) with free access to food and water. Mice were randomly distributed into two experimental groups of diet feeding: 1) regular chow/control diet (CD); and 2) HFD. The experimental protocol is depicted in Figure S1.

### Assessment of Energy Intake.

Mice were housed in groups of 2–4. HFD and chow diets were provided as pellets once a week. Energy intake was calculated by subtracting the amount of food leftover on any

given week from the amount of food given the previous week. This value was divided by the number of animals per cage. The amount of food (in grams) was then multiplied by the kcal/gram obtained from the manufacturer. The results were presented as Kcal consumed.

### Assessment of Energy Expenditure.

Oxylet gas analyzer and airflow unit (Oxylet; Panlab-Bioseb, Vitrolles, France) was used for the measurement of oxygen consumption ($\dot{V}O_2$) and carbon dioxide production ($VCO_2$). Mice were acclimated for 1 h daily for a week before measurements. The data for $VO_2$ are expressed as consumed volume of oxygen per minute per kilogram body weight ($ml \cdot min^{-1} \cdot kg^{-1}$).

### Micro-Computed Tomography (microCT) Scanning and Analysis.

Whole body microCT scans were obtained from mice anesthetized with isoflurane using the Quantum GX2 microCT imaging system (PerkinElmer Inc). Settings were optimized for body composition and CT scans were acquired for 6 minutes and analyzed using Analyze 14.0 software (AnalyzeDirect). Fat was isolated for analysis by density threshold. Separation of visceral and subcutaneous fat was done by sequential manual tracing of coronal slices in 2D, every 7 slices for the length of the ROI. Regions of similar density to fat were excluded using the same method to remove air within the lungs and equipment artifacts. The 3D sections were then reconstructed and processed to quantify volume. Fat free volume was calculated by subtracting total fat volume from total body volume (total body volume – (visceral fat volume + subcutaneous fat volume).

### Seahorse.

Frozen brown adipose tissue (BAT) samples were homogenized in 1X mitochondrial assay buffer (MAS) and mitochondrial extracts were prepared by sequential centrifugation. Mitochondrial extract (20 μg) was loaded into XFe 24 cell micro plate and centrifuged at 2,000xg for 20 minutes at 4°C. ADP (50 mmol/L); oligomycin (50 μmol/L); FCCP (50 μmol/L); antimycin A/rotenone (100 μmol/L/20 μmol/L) were prepared in 1X MAS buffer. Data is presented as fold-change from baseline respiration.

### Statistical Analysis.

Statistical comparisons were performed using ANOVA and *post-hoc* Tukey's test using Graph Pad Prism version 9.2.0 software. $P<0.05$ was considered to be significant. Energy expenditure data were also processed to analyze group and body size effects using ANCOVA. Figures are presented as dot plots indicating individual values with the mean and standard error of the mean (SEM).

A detailed description of methods and statistical analysis is included in a Supplementary File

## RESULTS

### Characterization of *Gpr75* null mice

*Gpr75*-deficient mice were viable and morphologically normal (1). *Gpr75* expression levels were undetectable in visceral fat from KO mice (Figure S2A) regardless of diet, while

expression levels of *Cyp4a12*, the murine 20-HETE synthase and major source for the GPR75 high-affinity ligand (8), were not different among the genotypes when fed chow diet but showed increases in response to HFD-feeding (Figure S2B). Plasma 20-HETE levels, which increased in response to HFD feeding (20, 21), did not differ among the genotypes (Figure S2C). On the other hand, plasma levels of CCL5, a reported low-affinity GPR75 ligand (8), were higher in HFD-fed WT mice compared to KO mice (Figure S2D). Importantly, blood pressure at baseline was similar in all genotypes. However, the increase in blood pressure associated with weight gain and 20-HETE-GPR75 pairing (7) was significantly attenuated in *Gpr75*-deficient mice (Figure S2E–F).

### *Gpr75* deletion attenuates HFD-driven weight gain

The initial body weights of all genotypes were comparable averaging 20.71±1.27 and 18.45±1.68 grams for males and females, respectively. Regular chow diet feeding for 14 weeks showed that all three genotypes gained similar amounts of weight averaging 5.74±0.12 and 5.16±0.13 grams for males and females respectively (Figure S3A–B). However, after 14 weeks of HFD feeding, each genotype diverged in weight accumulation, with male and female mice showing a similar degree of weight gain within all three genotypes, indicating an allele-dependent rate of weight gain (Figure 1A–B). Male WT mice more than doubled their weight (2.46-fold), while corresponding HET and KO mice added about 85% and 65% to their weight, respectively (Figure 1C). This pattern of weight gain was similar in female mice albeit the difference between the genotypes was more pronounced. Whereas female WT mice doubled their weight after HFD feeding, the HET and KO added only 50% and 14% to their weight, respectively, (Figure 1B and D).

Energy intake during HFD feeding was not significantly different between the genotypes of both sexes (Figure 1E–F; Figure S4). However, energy expenditure (EE) reduced by 25% in male and female WT animals after HFD-feeding and remained unchanged in KO mice in response to HFD-feeding regardless of sex (Figure 1G–H). Whereas EE reduced in male HET mice, it remained unchanged in female HET (Figure 1H). When placed on CD for 14 weeks, male and female WT, HET and KO mice showed no differences in weight gain, total energy intake or EE (Figure S3). Importantly, EE analyzed by ANCOVA using body weight or the volume of fat free tissue as covariates suggested that the differences in EE in response to HFD feeding are due to the genotype (Figures S5A and S5B). Regarding the decreased EE in WT, while it might be assumed that the newly acquired fat mass (vide infra) should increase energy expenditure, the increase in inflammatory myokines may negatively affect the bioenergetics of white adipose tissue. Hence, it is plausible that WT animals can gain fat mass, have stable, albeit dysfunctional, fat-free mass, and a drop in energy expenditure.

### *Gpr75* deletion reduces adiposity and adipocyte hypertrophy in response to HFD

Assessment of adipose tissue volume by microCT showed striking differences between the genotypes which were more prominent in female mice (Figure 2A–B). In male WT, the volume of visceral (VAT) and subcutaneous (SAT) adipose tissues increased by 9- and 12-fold in response to HFD feeding, respectively, whereas the increase in HET and especially in KO was largely attenuated compared to WT (Figure 2C–D). Similarly, VAT and SAT volume increased in HFD-fed female WT mice by 10 and 18-fold, respectively. In contrast, HET

female mice displayed attenuated increases amounting to 50% of that seen in WT, whereas VAT and SAT volume in female KO mice was largely unchanged (Figure 2E–F). Assessment of fat-free volume indicated no differences between WT and KO (Figure S6) which suggests that the increase in weight was primary due to increased fat volume.

Adipose tissue morphology also showed striking differences between WT and *Gpr75*-deficient mice. At baseline, all three genotypes showed similarities in adipocyte size in both males and females (Figure S7). However, following HFD feeding, adipocyte size from VAT and SAT of WT mice markedly increased, while adipocyte morphology from KO mice was largely unchanged (Figure 3A). Adipocyte size in VAT and SAT showed 3-fold increases in WT and no significant changes in KO mice (Figure 3B–E). Similarly, the size of VAT and SAT adipocytes from HFD-fed HET mice (not shown) was smaller than corresponding WT mice but significantly larger than corresponding KO mice, indicating allele-dependent protection from adipocyte hypertrophy. Histological sections of brown adipose tissue (BAT) showed striking morphological differences between WT and KO in response to HFD feeding; in WT, BAT contains large lipid droplets which in KO mice were much smaller and fewer in number for KO mice (Figure 3A).

### *Gpr75* deletion prevents HFD-driven hyperglycemia and insulin resistance

All genotypes showed the same levels of fasting blood glucose (FBS) at baseline (WT, HET and KO, respectively, 119±7, 120±7 and 125±9 mg/dL in male and 102±3, 99±3 and 100±3 mg/dL in female). In males, FBS significantly increased in all genotypes at weeks 7 and 14 of HFD feeding, although the increases were attenuated in HET and significantly so in KO mice; FBS levels after 14 weeks of HFD feeding were 232±7, 195±7 and 172±6 mg/dL for WT, HET and KO, respectively (Figures 4A and S10A). In females, WT and HET showed similar increases; however, KO mice experienced no hyperglycemia in response to HFD; FBS levels after HFD feeding were 167±4, 129±5 and 109±2 mg/dL for WT, HET and KO, respectively (Figures 4B and S10B).

To assess the ability to metabolize glucose, GTT was performed during HFD feeding. HFD-fed male and female WT mice showed a significant impairment of glucose tolerance (Figure S8). Assessment of area under the curve (AUC) clearly indicate the development of insulin resistance in both male and female WT mice (Figure 4C–D). Impairment in glucose tolerance was also seen in male and female HET and KO mice, although it was significantly attenuated in allele-dependent manner compared to WT mice (Figure 4C–D; Figures S8 and S10C–D). Insulin tolerance test showed a similar pattern. Impairment in glucose metabolism in response to insulin challenge was evident in both male and female WT mice and was largely absent in male and female HET and KO mice (Figure 4E–F; Figures S9 and S10E–F).

Plasma insulin, leptin and adiponectin were unchanged in all genotypes in response to CD feeding (Figure 5A–C). However, in response to HFD, levels of insulin and leptin in WT mice rose by 6- and 31-fold, respectively. Interestingly, in HET and KO mice the increase was attenuated in an allele-dependent manner. In HFD-fed HET, insulin and leptin rose by 2- and 14-fold, respectively, whereas in HFD-fed KO the increase amounted to 2- and 6-fold compared to corresponding mice on control diet (Figure 5A–B). Adiponectin levels were

higher in HFD-fed HET and KO by 51 and 58%, respectively, compared to corresponding mice on control diet and WT mice on HFD (Figure 5C). Resistin, which has been shown to increase in HFD-fed mice and correlate with the development of insulin resistance (23), also showed increased plasma levels in WT and HET but not in KO mice (Figure 5D). Likewise, levels of plasminogen activator inhibitor-1 (PAI-1) which has been characterized as a functional biomarker of metabolic syndrome (24) (25) displayed a 2-fold increase in response to HFD in WT but not in HET or KO mice (Figure 5E)

Measurements of HOMA-IR and leptin to adiponectin ratio (LAR), commonly used indices of insulin sensitivity (26), further indicated that *Gpr75* deficiency protects against the development of insulin resistance. Hence, HFD-fed WT mice displayed 3.5- and 7-fold higher HOMA-IR and LAR values than HFD-fed HET and KO mice (Figure 5F–G).

## *Gpr75* deletion increases expression of thermogenic genes while reducing HFD-driven inflammatory markers

Assessment of inflammatory genes and markers of mitochondria thermogenesis in VAT suggests that global *Gpr75* deletion negated HFD-driven inflammation while increasing thermogenesis. As seen in Figure 6A–C, in VAT from HFD-fed WT mice mRNA levels of *Il-6, Tnfα* and *Ccl5* increased by 1.5–2-fold when compared to corresponding WT mice on CD. The increase in inflammatory gene expression was largely absent in HFD-fed KO mice (Figure 6A–C). Interestingly, the expression of *Il-6, Tnfα* and *Ccl5* in 14-week CD-fed KO mice was significantly lower ($p<0.001$; Figure 6A–C) than corresponding WT, suggesting that *Gpr75* deficiency lowers the inflammatory milieu in visceral adipose tissue. Similar patterns were seen in SAT and BAT. Hence, levels of *Tnfα* mRNA increased by 2- and 6-fold in SAT and BAT of HFD-fed WT and was unchanged in HFD-fed KO (Figure 6I and 6L). It should be noted that at baseline, adipose tissue expression of inflammatory markers such as TNFα was not different among the genotypes (Figure S11A–C).

The expression of *Pgc1α*, a transcription factor and master regulator of mitochondrial biogenesis and insulin sensitivity which plays a critical role in the regulation of adipogenesis and in transforming WAT to brown fat-like adipocytes (27), significantly decreased in VAT (Figure 6D), but not in SAT and BAT, from HFD-fed WT mice (Figures 6G and 6J). In KO mice, the levels of *Pgc1α* mRNA in all adipose tissues were not significantly altered in response to HFD (Figure 6D), but in SAT and BAT the levels were significantly higher than the corresponding HFD-fed WT (Figures 6G and J).

We also measured expression of *Ucp1* (uncoupling protein 1), a thermogenic gene and a marker of BAT (28). At baseline, *Ucp1* expression was higher in KO adipose tissues than in WT (Figure S11D–F). After control diet feeding, *Ucp1* expression was 3–4-fold higher in SAT and BAT from KO mice compared to WT mice (Figures 6H and 6K). In response to HFD feeding, *Ucp1* expression in adipose tissues from WT mice was not different from control diet (Figures 6E, 6H and 6K). In contrast, HFD feeding caused significant changes in KO adipose tissues; in VAT, *Ucp1* levels increased by 3-fold (Figure 6E), in SAT there was a 50% decrease but the levels were still 4-fold higher than in corresponding WT (Figure 6H), and in BAT *Ucp1* levels, which after control diet feeding were 3-fold higher compared to WT, were unchanged in response to HFD (Figure 6K). The expression of

*Prdm16*, a transcriptional co-regulator and powerful inducer of the thermogenic phenotype of adipocytes (29), was measured in VAT tissues. It appeared that *Gpr75* deletion increased expression; however, it did not reach significance (Figure 6F). The response to HFD regarding the expression of these genes including *Ucp1*, *Pgc1a* and *Tnfa* was similar in males and females (Figure S12).

Western blot of UCP1 in BAT further indicated that the increase in *Ucp1* mRNA levels was associated with increased protein levels (Figure 7A). Moreover, assessment of BAT mitochondria function display significantly higher maximal respiration in response to ADP compared to mitochondria from WT BAT (Figure 7B), supporting, at least in part, the notion of increased thermogenic processes in KO mice when compared to WT mice under conditions of HFD feeding. In all, these results suggest that *Gpr75* deletion alters the characteristics of the HFD-driven adipose tissue phenotype, lowering the inflammatory milieu and favoring the reprogramming of white to beige (brown-like) adipose tissue (30). This notion of browning is taken carefully given the fact that the entire study was done in room temperature and not under conditions of thermoneutrality.

### Gpr75 deletion prevents HFD-mediated impairment in insulin signaling

We previously showed that 20-HETE, via activation of GPR75, inhibits insulin-mediated receptor phosphorylation at tyrosine 972, a key step in insulin-stimulated glucose uptake that has been shown to decrease in response to HFD in insulin-targeted tissues (20). In skeletal muscle, a prime insulin target, levels of *Gpr75* mRNA were undetectable in KO mice and were reduced by 50% in HET compared to WT (Figure 8A). Interestingly, expression of *Ucp3*, the uncoupling protein that is expressed in skeletal muscle and is associated with protection against diet-induced insulin resistance (31) was higher ($p<0.05$) in skeletal muscle from HFD-fed KO as compared to HFD-fed WT (Figure 8B). Moreover, expression of Mfn1, marker of mitochondrial function, was higher ($p<0.05$) in skeletal muscle from HFD-fed KO as compared to HFD-fed WT (Figure 8C). Lastly, the levels of phosphorylated insulin receptor (tyrosine 972) as well as phosphorylated AKT (serine 473), which is a primary target of activated insulin receptor, were elevated in skeletal muscle from HFD-fed KO as compared to corresponding WT (Figure 8D and 8E–F), suggesting that *Gpr75* deletion preserves insulin signaling and actions in response to HFD.

## DISCUSSION

The role of GPR75 in obesity and metabolic syndrome has become increasingly evident (1). A recent report indicated that *Gpr75* deficiency attenuates HFD-driven weight gain as a result of reduced food intake (32). Surprisingly, our study suggests that *Gpr75* deficiency protects against diet-induced obesity through effects on metabolic energy expenditure, rather than food intake. These differences may be due, at least in part, to differences in the genetic background which is known to influence the phenotypes of mutant mice (33). Hence, the genetic background of *Gpr75* null mice in the aforementioned report is C57BL/6JX129SV whereas the mice in our study are on C57Bl/6NTacXSW. Furthermore, we must acknowledge that in both studies animals were housed at controlled room temperature (20–24°C). Rodent metabolic studies may yield slightly different results at their thermoneutral

zone (29–31°C). Nevertheless, both studies show robust data linking protection from HFD-driven obesity in rodents. This protection was exemplified by attenuated hyperglycemia and sustained insulin sensitivity in an allele-dependent manner throughout the course of HFD feeding. While both male and female *Gpr75*-deficient mice showed similar trends of protection, the phenotype of female KO mice was undoubtedly more pronounced. This sex-difference merits further investigation.

Our data indicates that *Gpr75* null mice were no different from WT mice with respect to body weight or body fat composition at baseline. However, HFD-feeding caused attenuated weight gain in *Gpr75*-deficient mice compared to WT mice. The reduced weight gain correlates with reduced volume in adipose depots, particularly in SAT and VAT. Volume increase in VAT and SAT of WT mice was characterized by adipocyte hypertrophy. Moreover, BAT of WT mice shows enhanced lipid accumulation exemplified by large lipid droplets after HFD-feeding. Remarkably, *Gpr75*-deficient mice showed only a 25% increase in adipose volume and no indication of adipocyte hypertrophy or lipid accumulation. In fact, the morphology of all adipose tissues of KO mice after HFD feeding was similar to that observed at baseline and after CD feeding. These findings suggest that adipose tissues of KO mice are protected from excess lipid accumulation.

In exploring possible mechanisms that may underlie the protection *Gpr75* deletion affords against HFD-driven adiposity and insulin resistance, we turned to the biology of the GPR75 putative ligands. Both 20-HETE and CCL5 are potent inflammatory mediators. 20-HETE has been shown to activate the NF-kB inflammatory program and stimulate the production of cytokines and reactive oxygen species (34). It also stimulates neutrophil chemo-attraction (35). Likewise, CCL5 promotes adipose tissue inflammation through the recruitment of macrophages (36). Since inflammation is a key factor in the development of adiposity and adipocyte dysfunction in obesity (37, 38), it is reasonable to assume that the pairing of GPR75 with its ligands contributes to and promotes inflammation triggered by HFD. Numerous studies have shown the detrimental effects of adipose tissue inflammation on lipid handling. Expression of the proinflammatory cytokines *Il6* and *Tnfα* in VAT and SAT of WT animals shows a 2–6-fold increase after HFD-feeding. Remarkably, VAT, SAT, and BAT of KO animals did not show significant increases in pro-inflammatory cytokine expression after HFD-feeding. That adipocytes of HFD-fed KO mice are functionally healthier is also inferred from the levels of two adipokines in the plasma; levels of adiponectin, a key anti-inflammatory adipokine, were significantly higher, whereas levels of resistin, which have been associated with insulin resistance, were lower in KO mice as compared to corresponding WT.

While inflammation undoubtedly plays a key role in diet-induced obesity and adiposity, studies have highlighted the connection between BAT energy expenditure and obesity. A study by Ohno et al. (39) found that PPARγ ligands, particularly PRDM16, induce a brown fat gene program in subcutaneous white adipose to attenuate HFD-induced weight gain. Although, gene analysis of VAT, SAT, and BAT did not show significant changes in *Prdm16* between KO and WT mice after HFD-feeding, *Ucp1* expression decreased after HFD-feeding in WT animals in SAT and BAT. Surprisingly, *Ucp1* expression was significantly higher in SAT and BAT of KO animals compared to WT animals at baseline

and was not significantly reduced due to HFD-feeding. VAT of KO animals did not show any significant differences in *Ucp1* expression compared to WT animals. This may indicate that a UCP1-independent mechanism regulates thermogenesis in the VAT as is reported by Ikeda et al. (40). Furthermore, while HFD-feeding drove decreases in *Pgc1α* in WT adipose tissue depots, SAT and BAT of KO mice were totally protected. This suggests that mitochondrial function/homeostasis was maintained in the absence of *Gpr75*. Indeed, this notion was further supported by the demonstration of higher respiration rate in isolated mitochondria from BAT of HFD-fed KO compared to WT. 20-HETE has been shown to impair mitochondrial function through mechanisms that need further investigation (41, 42). However, it begs the question whether 20-HETE-mediated activation of GPR75 impacts adipocyte metabolic status.

Numerous studies have linked impaired glucose handling of obese individuals to alterations in insulin signaling. Goodyear et al. (43) reported that skeletal muscle from obese individuals had decreased phosphorylation of the insulin receptor, insulin receptor substrate-1, and phosphatidylinositol 3-kinase. Our data show that insulin receptor phosphorylation in skeletal muscle was maintained in HET and KO mice but not in WT mice after HFD-feeding. This correlates to reduced sensitivity to exogenous administration of insulin. Previously we showed that 20-HETE inhibits insulin-mediated insulin receptor phosphorylation *in vitro* and *in vivo* (20, 21). Moreover, treatment with 20-HETE receptor (GPR75) blockers prevented the 20-HETE-mediated inhibition of insulin signaling, suggesting that GPR75 is required for the 20-HETE effect (20). On the other hand, CCL5 has been shown to stimulate insulin secretion from beta-cells *in vitro* (4). However, its effect on insulin secretion *in vivo* is unknown. We have shown that while 20-HETE is a high-affinity ligand, CCL5 is a low affinity GPR75 ligand and its binding to GPR75 inhibits 20-HETE pairing with GPR75 (8). It is possible that during HFD, which induces the expression of 20-HETE producing enzymes, the excess and ability of 20-HETE to bind with high affinity overwhelmed the CCL5-GPR75 pairing. On the other hand, CCL5-GPR75 pairing may be the predominant interactions in beta cells and therefore may contribute to the hyperinsulinemia seen in HFD-fed WT mice. Additional studies are necessary to dissect the contribution of GPR75 and its ligands to the metabolic complications of obesity. Such studies should be directed towards development of conditional *Gpr75* knockout mice in targeting cells that contribute to the obese phenotype, e.g., beta cells and adipocytes.

While GPR75 has been identified as the high affinity 20-HETE receptor, others have demonstrated that the free fatty acid receptor FFAR1 (GPR40) is also a target for 20-HETE. Tunaru et al. (44), showed that 20-HETE binds to and activates GPR40 (albeit in much lower affinity than to GPR75, μM vs nM), which functions as an autocrine feed-forward regulator of glucose-stimulated insulin secretion. Although GPR40 is expressed primarily in pancreatic β-cells (44), the possibility exists that GPR40 tissue distribution and levels are altered/elevated in *Gpr75*-deficient mice, which may account for improved insulin sensitivity. The functional relationship between these two receptors is unknown and requires further investigation.

In summary, we provide strong evidence that GPR75 contributes to diet-induced adiposity and insulin resistance, possibly by impairing mitochondria function and insulin signaling.

This is inferred from results showing that *Gpr75*-deficient mice are protected from HFD-driven adiposity, hyperglycemia and insulin resistance. This is also deduced from the bioactions of the putative GPR75 ligands, namely 20-HETE and CCL5, which are known proinflammatory mediators having detrimental effects on mitochondrial function and insulin signaling.

## Supplementary Material

Refer to Web version on PubMed Central for supplementary material.

## Acknowledgement

We wish to thank the following medical students: Murad Elias and Dinusha Wanniarachchige for their help in conducting some of the studies described in this manuscript.

**FUNDING:**

This study was funded by NIH/NHLBI grant HL139793 (MLS) and a diversity supplement to Victor Garcia HL139793-1S.

## REFERENCES

1. Akbari P, Gilani A, Sosina O, Kosmicki JA, Khrimian L, Fang YY, et al. Sequencing of 640,000 exomes identifies GPR75 variants associated with protection from obesity. Science 2021;373. [PubMed: 34437096]
2. Dedoni S, Campbell LA, Harvey BK, Avdoshina V, Mocchetti I. The Orphan G Protein-coupled Receptor 75 Signaling is Activated by the Chemokine CCL5. J Neurochem 2018.
3. Ignatov A, Robert J, Gregory-Evans C, Schaller HC. RANTES stimulates Ca2+ mobilization and inositol trisphosphate (IP3) formation in cells transfected with G protein-coupled receptor 75. Br J Pharmacol 2006;149: 490–497. [PubMed: 17001303]
4. Liu B, Hassan Z, Amisten S, King AJ, Bowe JE, Huang GC, et al. The novel chemokine receptor, G-protein-coupled receptor 75, is expressed by islets and is coupled to stimulation of insulin secretion and improved glucose homeostasis. Diabetologia 2013;56: 2467–2476. [PubMed: 23979485]
5. Southern C, Cook JM, Neetoo-Isseljee Z, Taylor DL, Kettleborough CA, Merritt A, et al. Screening beta-arrestin recruitment for the identification of natural ligands for orphan G-protein-coupled receptors. J Biomol Screen 2013;18: 599–609. [PubMed: 23396314]
6. Davenport AP, Alexander SP, Sharman JL, Pawson AJ, Benson HE, Monaghan AE, et al. International Union of Basic and Clinical Pharmacology. LXXXVIII. G protein-coupled receptor list: recommendations for new pairings with cognate ligands. Pharmacol Rev 2013;65: 967–986. [PubMed: 23686350]
7. Garcia V, Gilani A, Shkolnik B, Pandey V, Zhang FF, Dakarapu R, et al. 20-HETE Signals Through G-Protein-Coupled Receptor GPR75 (Gq) to Affect Vascular Function and Trigger Hypertension. Circ Res 2017;120: 1776–1788. [PubMed: 28325781]
8. Pascale JV, Park EJ, Adebesin AM, Falck JR, Schwartzman ML, Garcia V. Uncovering the signaling, structure and function of the 20-HETE-GPR75 pairing: Identifying CCL5 as a negative regulator of GPR75. Br J Pharmacol 2021.
9. Theken KN, Deng Y, Schuck RN, Oni-Orisan A, Miller TM, Kannon MA, et al. Enalapril reverses high-fat diet-induced alterations in cytochrome P450-mediated eicosanoid metabolism. American journal of physiology Endocrinology and metabolism 2012;302: E500–509. [PubMed: 22185841]
10. Joseph G, Soler A, Hutcheson R, Hunter I, Bradford C, Hutcheson B, et al. Elevated 20-HETE impairs coronary collateral growth in metabolic syndrome via endothelial dysfunction. Am J Physiol Heart Circ Physiol 2017;312: H528–H540. [PubMed: 28011587]

11. Tsai IJ, Croft KD, Mori TA, Falck JR, Beilin LJ, Puddey IB, et al. 20-HETE and F2-isoprostanes in the metabolic syndrome: the effect of weight reduction. Free Radic Biol Med 2009;46: 263–270. [PubMed: 19013235]
12. Issan Y, Hochhauser E, Guo A, Gotlinger KH, Kornowski R, Leshem-Lev D, et al. Elevated level of pro-inflammatory eicosanoids and EPC dysfunction in diabetic patients with cardiac ischemia. Prostaglandins Other Lipid Mediat 2013;100–101: 15–21.
13. Auguet T, Aragones G, Colom M, Aguilar C, Martin-Paredero V, Canela N, et al. Targeted metabolomic approach in men with carotid plaque. PloS one 2018;13: e0200547.
14. Soler A, Hunter I, Joseph G, Hutcheson R, Hutcheson B, Yang J, et al. Elevated 20-HETE in metabolic syndrome regulates arterial stiffness and systolic hypertension via MMP12 activation. Journal of molecular and cellular cardiology 2018;117: 88–99. [PubMed: 29428638]
15. Pauley M, Mays C, Bailes JR, Schwartzman ML, Castle M, McCoy M, et al. Carbohydrate-Restricted Diet: A Successful Strategy for Short-Term Management in Youth with Severe Obesity-An Observational Study. Metab Syndr Relat Disord 2021.
16. Kim DH, Puri N, Sodhi K, Falck JR, Abraham NG, Shapiro J, et al. Cyclooxygenase-2 dependent metabolism of 20-HETE increases adiposity and adipocyte enlargement in mesenchymal stem cell-derived adipocytes. J Lipid Res 2013;54: 786–793. [PubMed: 23293373]
17. Zoccali C, Mallamaci F, Grassi G. 20-Hydroxyeicosatetraenoic acid, a far-reaching autacoid in chronic kidney disease: hypertension and beyond. J Hypertens 2015;33: 1764–1766. [PubMed: 26244625]
18. Wang Z, Yadav AS, Leskova W, Harris NR. Inhibition of 20-HETE attenuates diabetes-induced decreases in retinal hemodynamics. Exp Eye Res 2011;93: 108–113. [PubMed: 21658386]
19. Li X, Zhao G, Ma B, Li R, Hong J, Liu S, et al. 20-Hydroxyeicosatetraenoic acid impairs endothelial insulin signaling by inducing phosphorylation of the insulin receptor substrate-1 at Ser616. PloS one 2014;9: e95841.
20. Gilani A, Agostinucci K, Hossain S, Pascale JV, Garcia V, Adebesin AM, et al. 20-HETE interferes with insulin signaling and contributes to obesity-driven insulin resistance. Prostaglandins Other Lipid Mediat 2020;152: 106485.
21. Gilani A, Pandey V, Garcia V, Agostinucci K, Singh SP, Schragenheim J, et al. High-fat diet-induced obesity and insulin resistance in CYP4a14(−/−) mice is mediated by 20-HETE. Am J Physiol Regul Integr Comp Physiol 2018;315: R934–r944. [PubMed: 30088983]
22. Lai G, Wu J, Liu X, Zhao Y. 20-HETE induces hyperglycemia through the cAMP/PKA-PhK-GP pathway. Molecular endocrinology (Baltimore, Md) 2012;26: 1907–1916. [PubMed: 22918876]
23. Steppan CM, Lazar MA. Resistin and obesity-associated insulin resistance. Trends Endocrinol Metab 2002;13: 18–23. [PubMed: 11750858]
24. Juhan-Vague I, Alessi MC, Mavri A, Morange PE. Plasminogen activator inhibitor-1, inflammation, obesity, insulin resistance and vascular risk. J Thromb Haemost 2003;1: 1575–1579. [PubMed: 12871293]
25. Levine JA, Oleaga C, Eren M, Amaral AP, Shang M, Lux E, et al. Role of PAI-1 in hepatic steatosis and dyslipidemia. Scientific reports 2021;11: 430. [PubMed: 33432099]
26. Hung AM, Sundell MB, Egbert P, Siew ED, Shintani A, Ellis CD, et al. A comparison of novel and commonly-used indices of insulin sensitivity in African American chronic hemodialysis patients. Clin J Am Soc Nephrol 2011;6: 767–774. [PubMed: 21441124]
27. Puigserver P, Spiegelman BM. Peroxisome proliferator-activated receptor-gamma coactivator 1 alpha (PGC-1 alpha): transcriptional coactivator and metabolic regulator. Endocr Rev 2003;24: 78–90. [PubMed: 12588810]
28. Fedorenko A, Lishko PV, Kirichok Y. Mechanism of fatty-acid-dependent UCP1 uncoupling in brown fat mitochondria. Cell 2012;151: 400–413. [PubMed: 23063128]
29. Chi J, Cohen P. The Multifaceted Roles of PRDM16: Adipose Biology and Beyond. Trends Endocrinol Metab 2016;27: 11–23. [PubMed: 26688472]
30. Lee Y-H, Mottillo EP, Granneman JG. Adipose tissue plasticity from WAT to BAT and in between. Biochimica et biophysica acta 2014;1842: 358–369. [PubMed: 23688783]
31. Chan CB, Harper ME. Uncoupling proteins: role in insulin resistance and insulin insufficiency. Current diabetes reviews 2006;2: 271–283. [PubMed: 18220632]

32. Powell DR, Doree DD, DaCosta CM, Platt KA, Brommage R, Buhring L, et al. Mice Lacking Gpr75 are Hypophagic and Thin. Diabetes Metab Syndr Obes 2022;15: 45–58. [PubMed: 35023939]
33. Doetschman T Influence of genetic background on genetically engineered mouse phenotypes. Methods Mol Biol 2009;530: 423–433. [PubMed: 19266333]
34. Hoopes SL, Garcia V, Edin ML, Schwartzman ML, Zeldin DC. Vascular actions of 20-HETE. Prostaglandins Other Lipid Mediat 2015;120: 9–16. [PubMed: 25813407]
35. Tsai IJ, Croft K, Puddey IB, Beilin LJ, Barden AE. 20-Hydroxyeicosatetraenoic Acid Synthesis Is Increased in Human Neutrophils and Platelets by Angiotensin Ii and Endothelin-1. Am J Physiol Heart Circ Physiol 2011;300: H1194–1200. [PubMed: 21239640]
36. Keophiphath M, Rouault C, Divoux A, Clément K, Lacasa D. CCL5 promotes macrophage recruitment and survival in human adipose tissue. Arterioscler Thromb Vasc Biol 2010;30: 39–45. [PubMed: 19893003]
37. Lee BC, Lee J. Cellular and molecular players in adipose tissue inflammation in the development of obesity-induced insulin resistance. Biochim Biophys Acta 2014;1842: 446–462. [PubMed: 23707515]
38. Suganami T, Ogawa Y. Adipose tissue macrophages: their role in adipose tissue remodeling. J Leukoc Biol 2010;88: 33–39. [PubMed: 20360405]
39. Ohno H, Shinoda K, Spiegelman BM, Kajimura S. PPARγ agonists induce a white-to-brown fat conversion through stabilization of PRDM16 protein. Cell Metab 2012;15: 395–404. [PubMed: 22405074]
40. Ikeda K, Kang Q, Yoneshiro T, Camporez JP, Maki H, Homma M, et al. UCP1-independent signaling involving SERCA2b-mediated calcium cycling regulates beige fat thermogenesis and systemic glucose homeostasis. Nat Med 2017;23: 1454–1465. [PubMed: 29131158]
41. Cui W, Wu X, Shi Y, Guo W, Luo J, Liu H, et al. 20-HETE synthesis inhibition attenuates traumatic brain injury-induced mitochondrial dysfunction and neuronal apoptosis via the SIRT1/PGC-1α pathway: A translational study. Cell Prolif 2021;54: e12964.
42. Lakhkar A, Dhagia V, Joshi SR, Gotlinger KH, Patel D, Sun D, et al. 20-HETE-Induced Mitochondrial Superoxide and Inflammatory Phenotype in Vascular Smooth Muscle is Prevented by Glucose-6-Phosphate Dehydrogenase Inhibition. Am J Physiol Heart Circ Physiol 2016;310: H1107–1117. [PubMed: 26921441]
43. Goodyear LJ, Giorgino F, Sherman LA, Carey J, Smith RJ, Dohm GL. Insulin receptor phosphorylation, insulin receptor substrate-1 phosphorylation, and phosphatidylinositol 3-kinase activity are decreased in intact skeletal muscle strips from obese subjects. J Clin Invest 1995;95: 2195–2204. [PubMed: 7537758]
44. Tunaru S, Bonnavion R, Brandenburger I, Preussner J, Thomas D, Scholich K, et al. 20-HETE promotes glucose-stimulated insulin secretion in an autocrine manner through FFAR1. Nature communications 2018;9: 177.

- What is already known about this subject?

  The orphan G-protein-coupled receptor *GPR75* has been identified as a novel obesity gene and its putative high-affinity ligand, 20-hydroxyeicosatetraenoic acid (20-HETE), is a pro-inflammatory and adipogenic lipid mediator. Deletion of *Gpr75* in mice attenuates high fat-diet driven weight gain and hyperglycemia.

- What are the new findings?

  Here we show that deletion of *Gpr75* in mice prevents diet-driven adiposity, adipocyte hypertrophy and insulin resistance. We further provide evidence that this protection is possibly accounted for by reduction of inflammation and preservation of mitochondria function and insulin signaling.

- How might the results change the direction of research or the focus of clinical practice?

  *GPR75* is a novel obesity gene whose mechanism of action is yet to be explored. Its targeting may present a novel strategy to combat obesity-driven cardiometabolic diseases. Understanding the mechanisms underlying GPR75's contribution to obesity is paramount to any drug development.

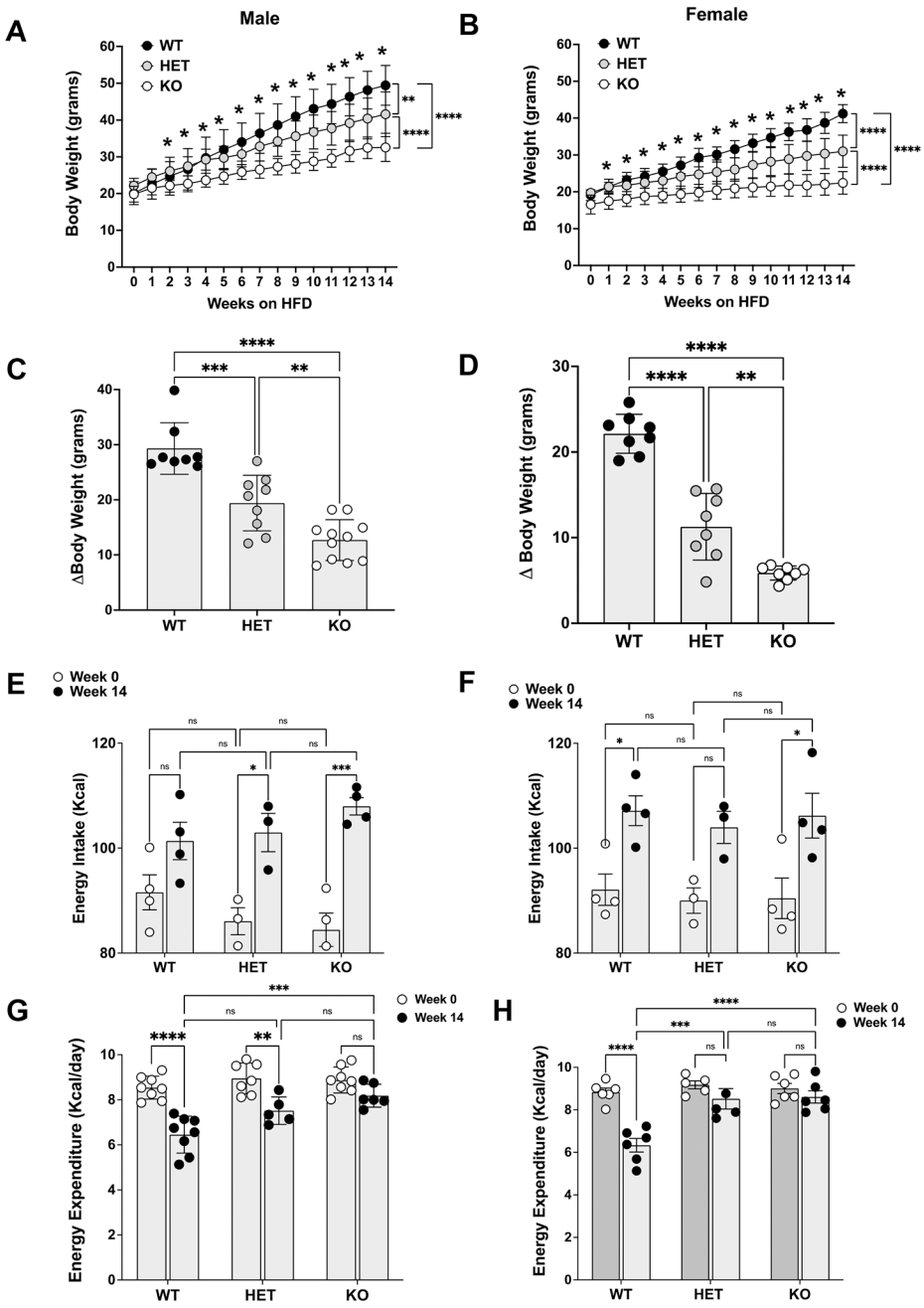


**Figure 1: Body weight, energy intake, and energy expenditure over 14-weeks of HFD.**

Body weight trajectories for (**A**) male (n=8–11), and (**B**) female (n=7–8) WT, HET and KO mice. Results are mean±SE; n=8–11/group; *p=0.05 from WT by unpaired T-Test. Change in body weight from baseline after 14 weeks of HFD feeding for males (**C**) and females (**D**). Total energy intake before and after HFD feeding for (**E**) male and (**F**) female WT, HET, and KO mice. Energy expenditure (Kcal/day) at baseline and week 14 of HFD feeding for (**G**) males and (**H**) females. Results are mean±SE, ns, not significant; **p<0.01, *** P<0.001 and ****p<0.0001 by two-way ANOVA with Tukey's multiple comparison test.

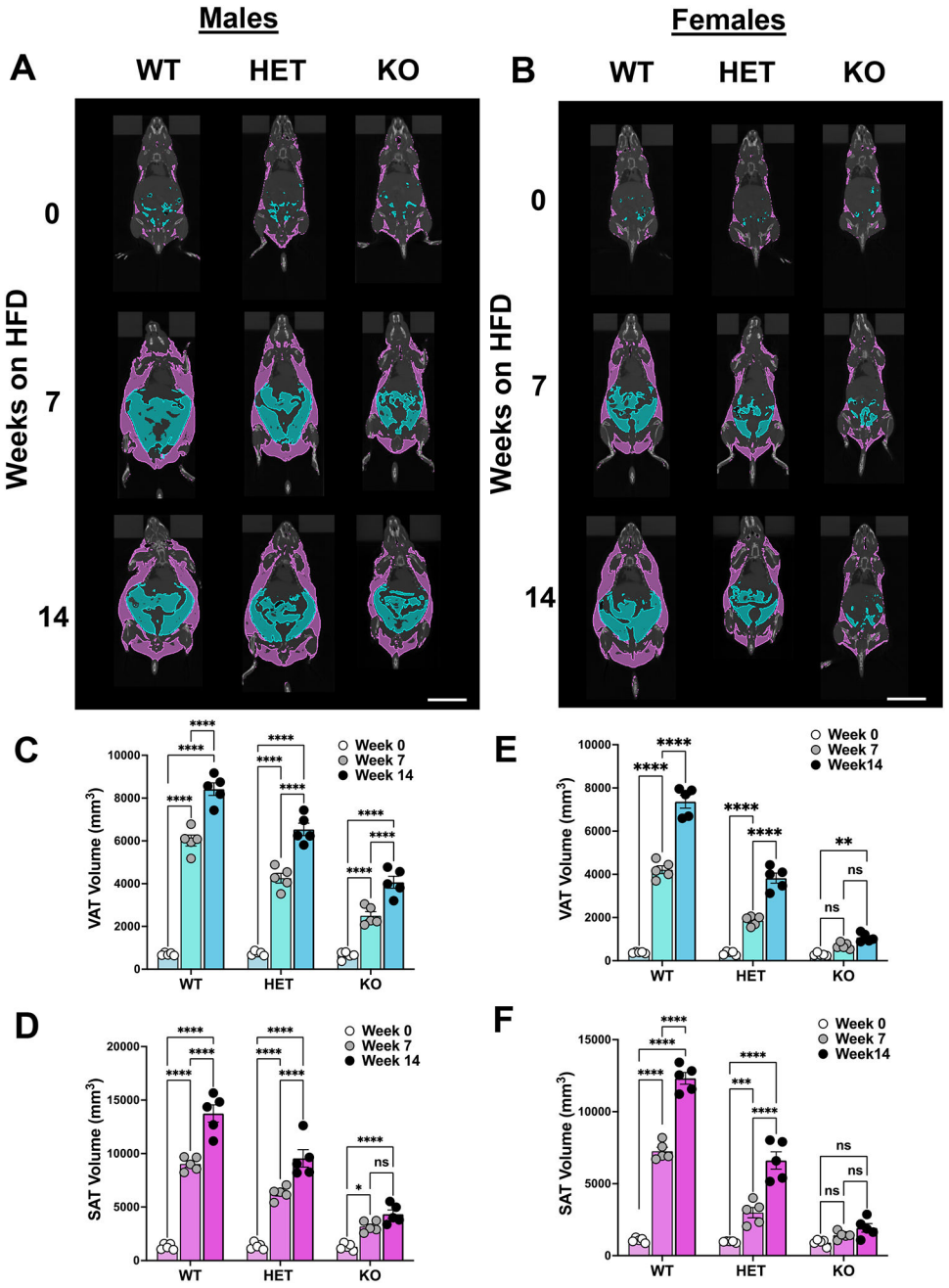


**Figure 2: Visceral and subcutaneous fat pad composition over 14-weeks of HFD.**

Representative MicroCT images of male (**A**) and female (**B**) WT, HET and KO mice at weeks 0, 7 and 14 of HFD feeding (blue, visceral fat; purple, subcutaneous fat; scale bar = 20 mm). Visceral (VAT) and subcutaneous (SAT) fat volumes at baseline, week 7, and week 14 for males (**C-D**) and females (**E-F**) WT, HET and KO mice. Results are mean±SE, ns, not significant; **p<0.01, *** P<0.001 and ****p<0.0001 by two-way ANOVA with Tukey's multiple comparison test.

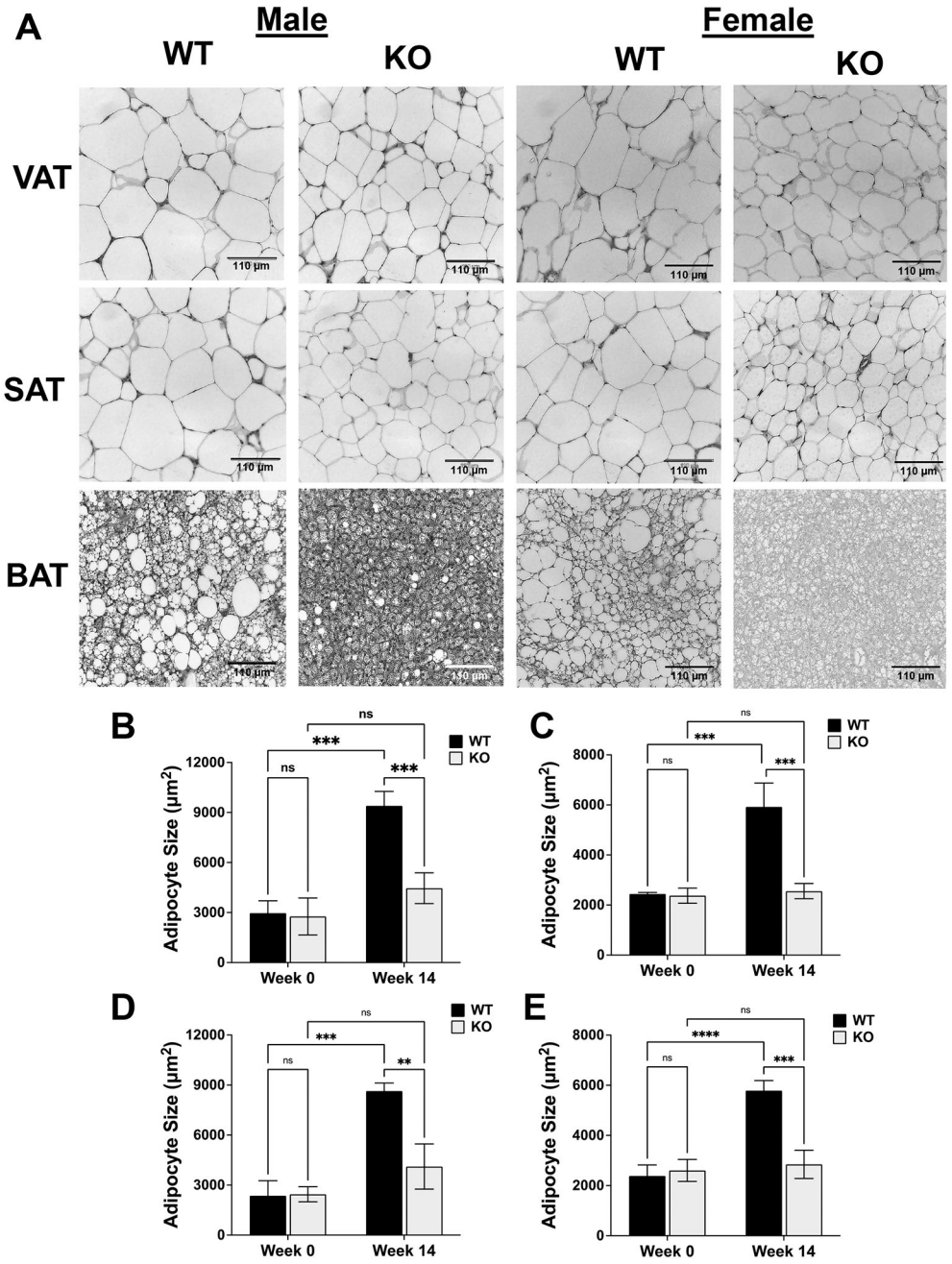


**Figure 3: Visceral, subcutaneous, and brown fat morphology after 14-weeks of HFD.**

(**A**) Representative images of H&E staining in visceral (VAT), subcutaneous (SAT) and brown (BAT) adipose tissues of HFD (14 weeks)-fed male and female WT and KO mice (20X; scale bar = 110 µm). Visceral adipocyte size at baseline and week 14 of HFD for males (**B**) and females (**C**). Subcutaneous adipocyte size at baseline and week 14 of chow diet or HFD for males (**D**) and females (**E**). Results are mean±SE (n=4); ns, not significant; **p<0.01, *** P<0.001 and ****p<0.0001 by two-way ANOVA with Tukey's multiple comparison test.

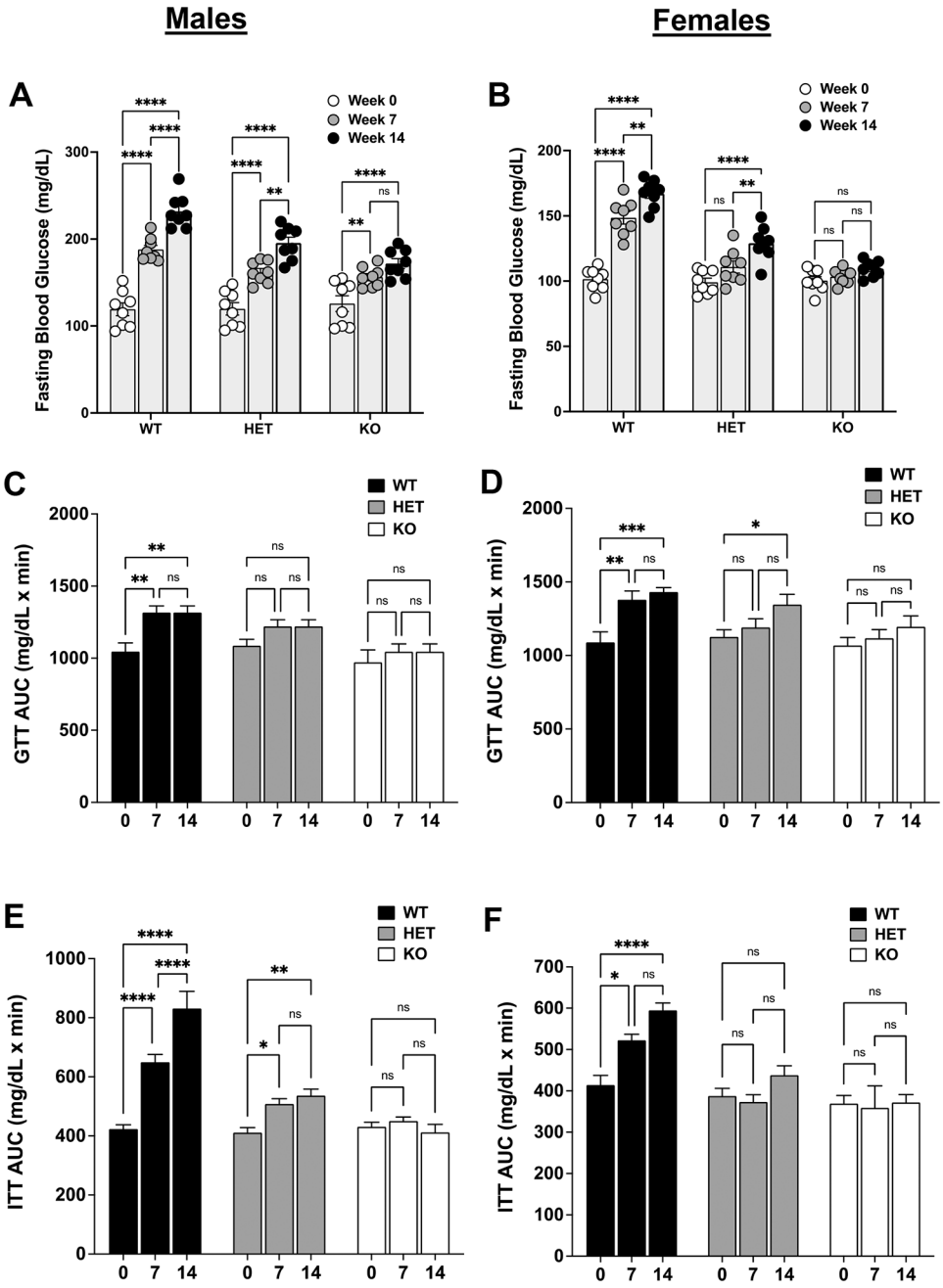


**Figure 4: Fasting blood glucose, glucose tolerance, and insulin tolerance over 14-weeks of HFD.**

Twelve-hour fasting blood glucose of (**A**) males and (**B**) female WT, HET, and KO mice at weeks 0, 7 and 14 of HFD feeding. Glucose tolerance test (GTT) area under curve (AUC) of (**C**) males and (**D**) female WT, HET, and KO mice at weeks 0, 7 and 14 of HFD feeding. Insulin tolerance test (ITT) area under curve (AUC) of (**E**) males and (**F**) female WT, HET, and KO mice at weeks 0, 7 and 14 of HFD feeding. Results are mean±SE (n=8); ns, not significant; **p<0.01, *** P<0.001 and ****p<0.0001 by two-way ANOVA with Tukey's multiple comparison test.

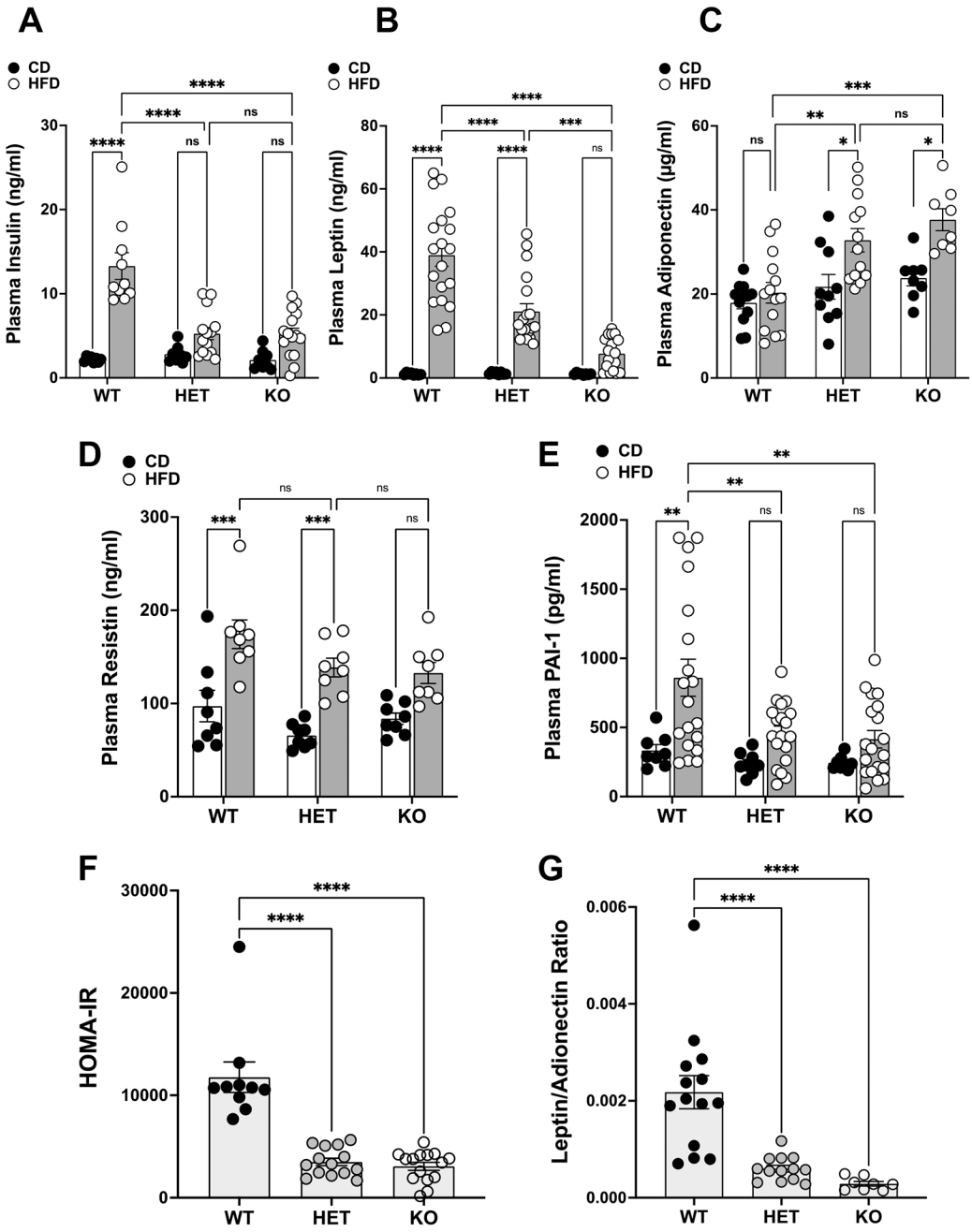


**Figure 5: Levels of markers of insulin resistance in response to diet.**

Plasma insulin (**A**), leptin (**B**), adiponectin (**C**), resistin (**D**) and PAI-1 (**E**) after 14 weeks of chow diet (CD) or HFD feeding in WT, HET and KO mice. (**F**) Homeostatic model assessment of insulin resistance (HOMA-IR) after 14 weeks of HFD-feeding. (**G**) Leptin-adiponectin ratio after 14 weeks of HFD feeding. Results are mean±SE (n=10–20); ns, not significant; **p<0.01, *** P<0.001 and ****p<0.0001 by two-way ANOVA with Tukey's multiple comparison test.

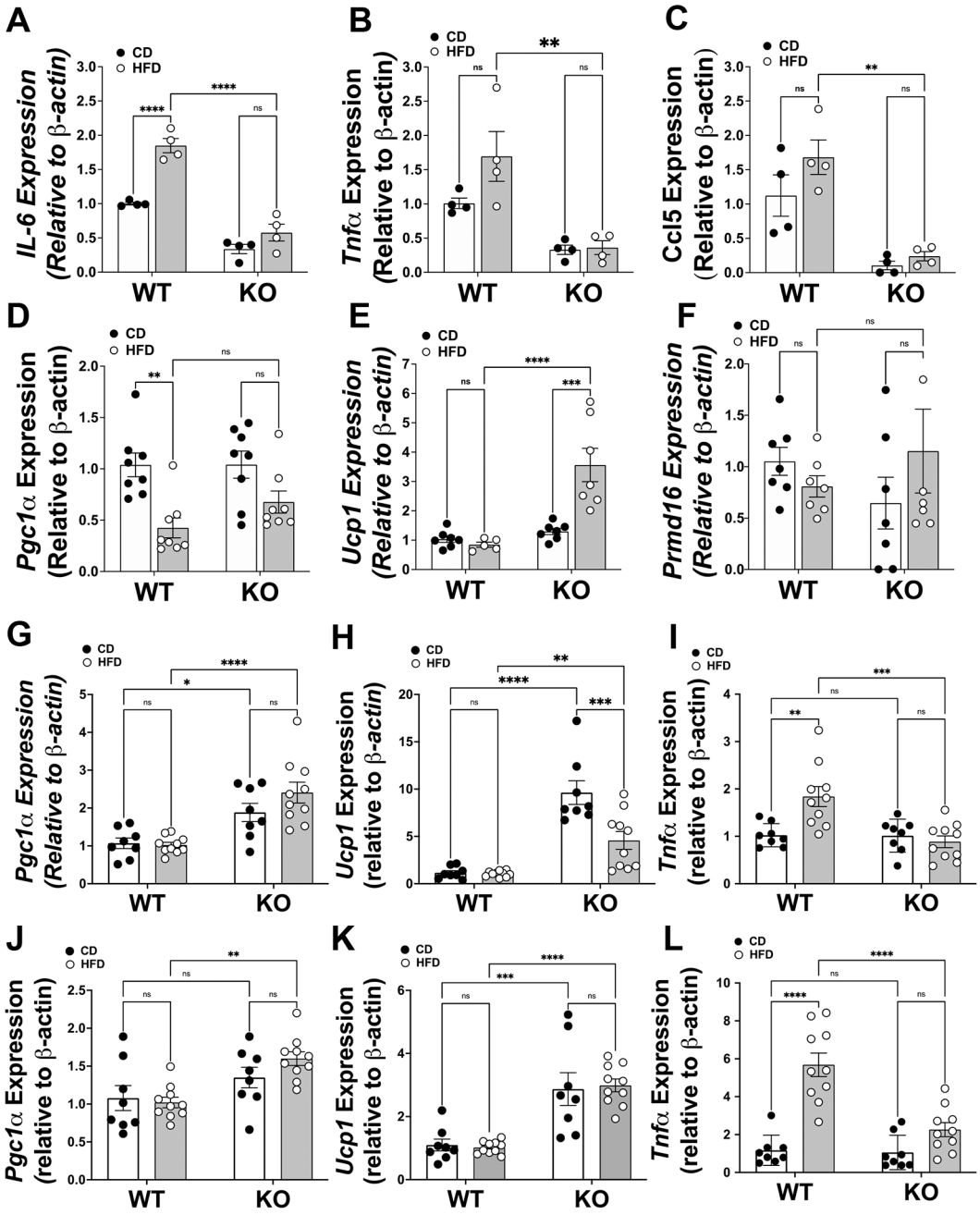


**Figure 6: Expression of inflammatory and thermogenic markers in adipose tissues.**

Levels of mRNA of **(A)** interleukin-6 (*Il-6*), (**B**) tumor necrosis factor-alpha (*Ucp1*), (**C**) chemokine ligand 5 (*Ccl5*), (**D**) peroxisome proliferator-activated receptor gamma coactivator 1-alpha (*Pgc1α*), (**E**) uncoupling protein-1 (*Ucp1*) and (**F**) PR domain containing 16 (*Prmd16*) in VAT of WT and KO mice after 14 weeks of chow diet (CD) or HFD feeding. Expression of *Pgc1α* (**G**) *Ucp1* (**H**) and *Ucp1* (**I**) in subcutaneous (SAT) of WT and KO animals after 14 weeks of chow diet (CD) or HFD-feeding. Expression of *Pgc1α* (**J**) *Ucp1* (**K**) and *Ucp1* (**L**) in BAT of WT and KO animals after 14 weeks of chow diet (CD) or HFD-feeding. Results are mean±SE (n=8–10); ns, not significant; *p<0.05,

**p<0.01, *** P<0.001 and ****p<0.0001 by two-way ANOVA with Tukey's multiple comparison test.

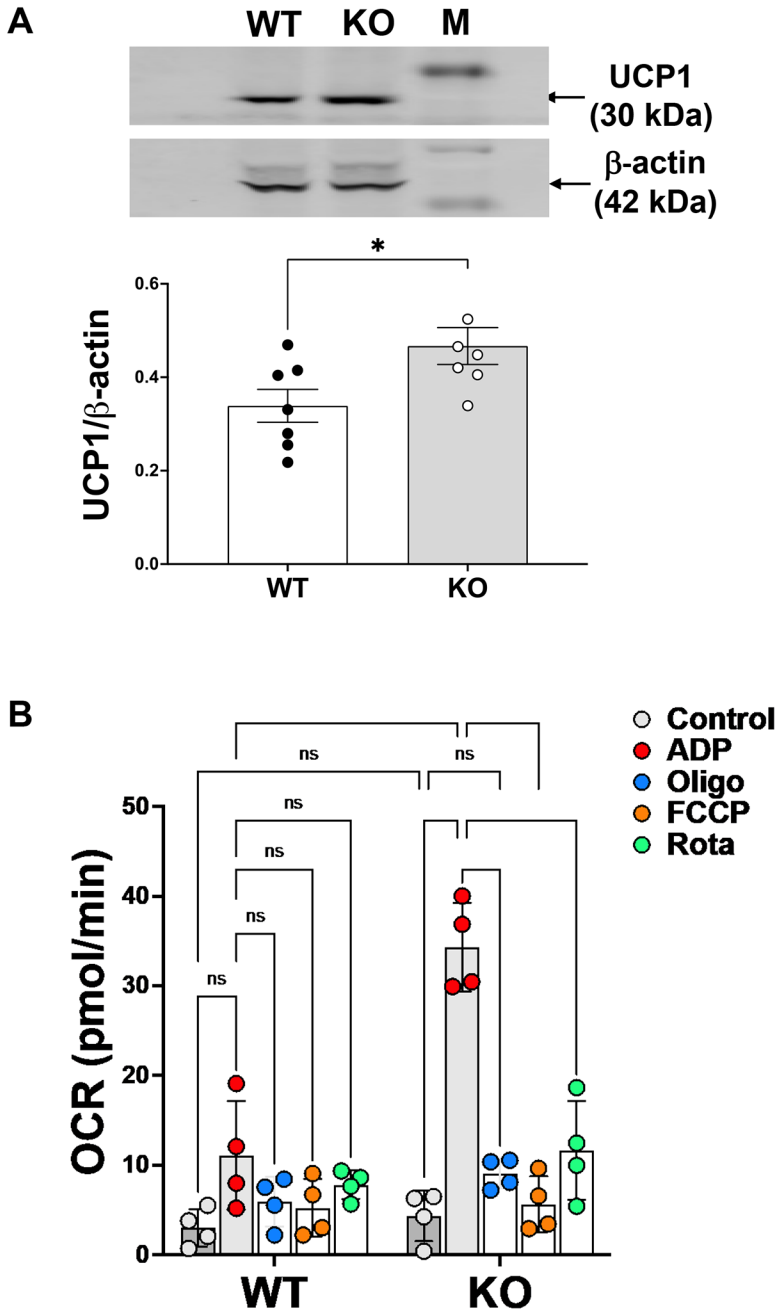


**Figure 7: UCP1 protein levels and mitochondria respiration in BAT from HFD-fed WT and KO mice.**

(**A**) Western blot and densitometry analysis of UCP1 in BAT from WT and KO mice after 14 weeks of HFD feeding. Results are mean±SE, n=6/group; *p<0.05 compared to WT by unpaired T-Test. (B) ADP-stimulated oxygen respiration in isolated mitochondria from BAT of WT and KO mice after 14 weeks of HFD feeding. Results are mean±SE, n=4/group, ****p<0.0001 by two-way ANOVA with Tukey's multiple comparison test.

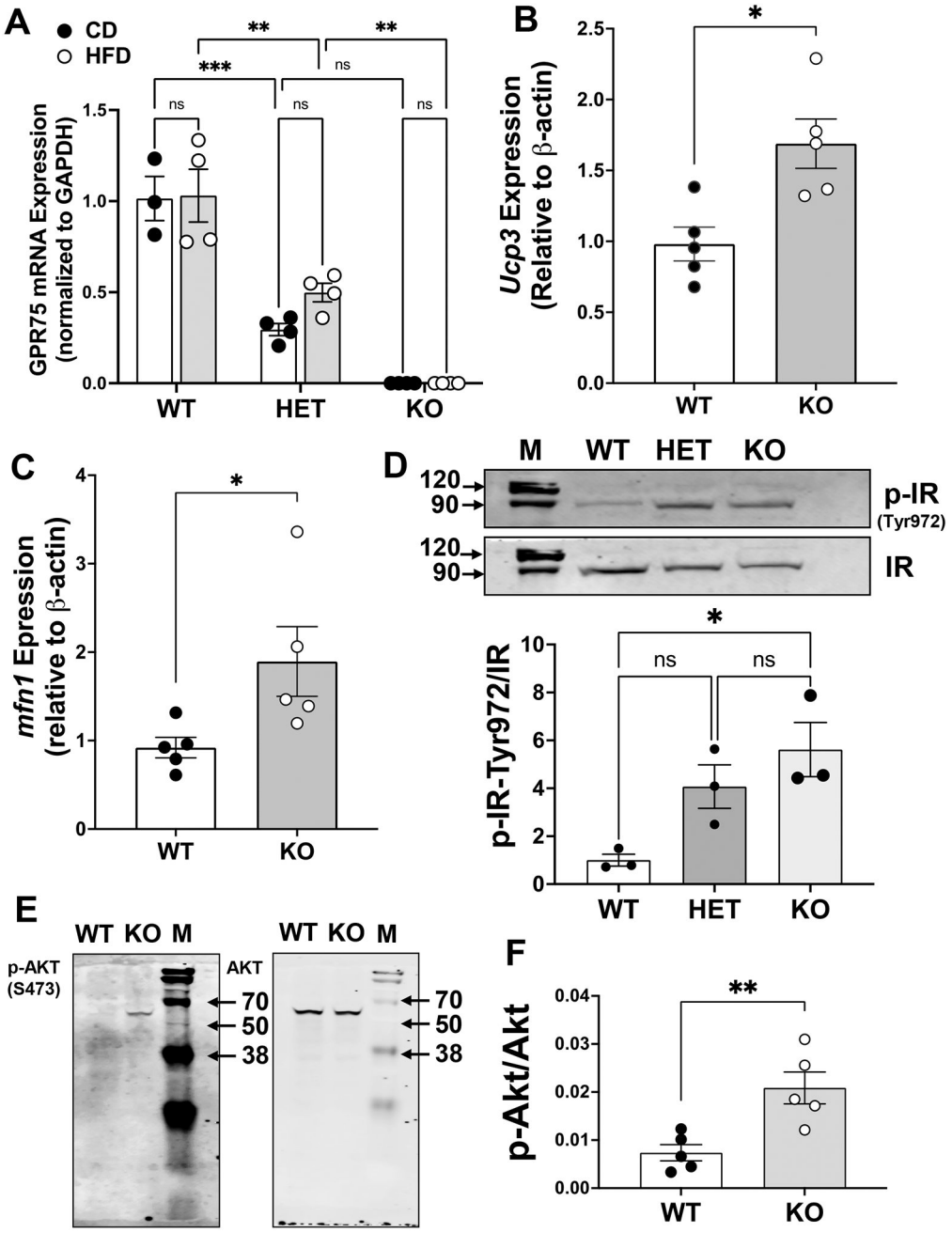


**Figure 8: Skeletal muscle thermogenic marker expression and insulin signaling.**

(**A**) *Gpr75* gene expression in WT, HET and KO mice after 14 weeks of chow diet (CD) or HFD-feeding. (**B**) Expression levels of uncoupling protein-3 (*Ucp3*) and (**C**) Mitofusin-1 (*Mfn1*) in WT and KO after 14 weeks of CD- or HFD-feeding. (**D**) representative western blot and densitometry analysis of phosphorylated insulin receptor at tyrosine 972 (pIR) normalized to total insulin receptor (IR) levels in skeletal muscle from HFD-fed WT, HET, and KO mice. (**E**) western blot and (**F**) densitometry analysis of phospho-AKT (serin 473) normalized to total AKT in skeletal muscle from HFD-fed WT and KO mice. Results are

mean±SE (n=3–5); ns, not significant; *p<0.05, **p<0.01, *** P<0.001 by unpaired t-test (B, C and E) or two-way ANOVA with Tukey's multiple comparison test (A and D).